The International Journal of Advanced Manufacturing Technology (2019) 101:1467–1479
https://doi.org/10.1007/s00170-018-2929-2

ORIGINAL ARTICLE

Study on grinding force model in ultrasonic vibration-assisted grinding of alloy structural steel

Deguo Li[1] · Jinyuan Tang[1] · Haifeng Chen[1,2] · Wen Shao[1]

Received: 2 May 2018 / Accepted: 23 October 2018 / Published online: 21 November 2018

Abstract

Based on the micro-removal mechanism of the ultrasonic vibration-assisted grinding (UVAG), a new prediction model of alloy structural steel is proposed in this paper. In the grinding process, the abrasive grains mainly go through two stages: plowing stage and chip forming stage. Then, grinding force model of single grain under different material removal modes is established. The thickness of the abrasive grain, the number of grains involved in grinding, and the interference between the abrasive grains are essential factors that affect the grinding force. Considering the influence of ultrasonic vibration on these factors, the grinding force model of the grinding wheel is developed. The ultrasonic grinding experiments are conducted to validate this model. Findings show that the theoretically predicted results are consistent with the experimental results.

Keywords Ultrasonic grinding · Chip thickness · Plowing · Chip forming · Grinding force

Nomenclature

d_s	Wheel diameter
b	Grinding width
n_s	Grinding wheel speed
a_p	Grinding depth
v_w	Work speed
A	Ultrasonic amplitude
f	Ultrasonic frequency
ϕ_c	Angle between the movement direction of the grain and the main cutting direction
L	Interval of two continuous cutting edges
s	Workpiece translation within adjacent grain intervals
l_c	Chip forming length
t_p	Single grain plowing time
t_c	Cutting time
l_p	Plowing length
V_{uc}	Removed workpiece material volume by single grain
N_a	Number of active grains
γ_0	Grain half vertex angle
F_{px}, F_{py}	Plowing normal force and tangential force of single abrasive grain
μ_p, μ_c	Plowing and cutting friction coefficients
A_p	Plowing area
A_D	Sectional area of cutting layer
A_s	Sectional area of shear plane
δ_p	Yield stress of workpiece
τ_s	Shear stress of workpiece
$F_{cx}F_{cy}$	Grinding normal force and tangential force of single grain
λ	Ultrasonic wavelength
l_{k1}, l_{k2}	Two adjacent abrasive cutting lengths
l_{k1-1}, l_{k1-2}	Interference and non-interference lengths
β	Friction angle
ϕ	Shear angle
m	Number of interferences
n	Interference period
d_{gmin}	Minimum grain diameter
d_{gmax}	Maximum grain diameter
d_{gmean}	Average grain diameter
N_p,N_c	Number of grains in plowing and cutting forming contact zone
F_n, F_t	

✉ Jinyuan Tang
jytangcsu_312@163.com

[1] State Key Laboratory of High Performance Complex Manufacturing, Central South University, Changsha 410083, China

[2] Hunan Provincial Key Laboratory of High Efficiency and Precision Machining of Difficult-to-Cut Materials, Hunan University of Science and Technology, Xiangtan 411201, Hunan, China

Ultrasonic grinding normal force and tangential force in grinding zone

1 Introduction

As a compound processing technology with ultrasonic vibration added in the grinding process, ultrasonic vibration-assisted grinding (UVAG) has been widely used in difficult-to-cut material because it can reduce grinding force, decrease grinding temperature, and improve the surface quality of workpiece [1–8]. The grinding force, one of the most important physical quantities to describe the grinding mechanism, reflects the interaction between the grinding wheel and the workpiece in the grinding zone and directly relates to the removal mechanism of the material in the grinding process and the grinding quality of the workpiece [9]. Therefore, research on grinding force remains an important method to understand the mechanism of ultrasonic grinding.

At present, many scholars have focused on the modeling of ultrasonic grinding force, especially in hard and brittle materials. Liu et al. [10] considered that the removal of brittle materials was achieved through the brittle fracture. Based on fracture mechanics, the grinding force model of ultrasonic vibration was originally established along the radial direction of the grinding wheel. The change of grinding force under different parameters was analyzed and verified by experiments. Based on the motion characteristics of ultrasonic machining and the fracture characteristics of brittle materials, Wang et al. [11] calculated the critical ultrasonic frequency and amplitude of the single grain movement track where no interference was produced and explained the reasons why the grinding force was reduced and the grinding quality was improved under the ultrasonic grinding. Ning et al. [12] calculated the removal of carbon fiber composites by rotating ultrasonic machining based on brittle fracture mechanism and established the mechanical model of cutting force in the feed direction. The fracture volume coefficient of the workpiece material was obtained through experiments. Cong et al. [13] argued that brittle fracture was the main removal mode of carbon fiber composites. By calculating the indentation depth, effective contact time, and maximum impact force of grains in ultrasonic processing, the cutting force model of carbon fiber composites with rotary ultrasonic machining was developed. The abovementioned grinding force models are all based on the assumption that the material is removed by means of brittle fracture. However, there is more than one mode of material removal in ultrasonic grinding.

The main removal mode of material is the basis for establishing the model of ultrasonic grinding force. With the increasing understanding of material removal methods, new progress has been made in the modeling of ultrasonic grinding force. Li et al. [14] carried out a varied depth nano-scratch test of single grain. The results show that the material removal of SiC has four distinctive stages, including plastic deformation without chips, ductile removal, brittle-to-ductile transition, and brittle removal. Based on the relationship between the grinding force and the length and depth of the crack, the theoretical model of the ultrasonic grinding force of the SiC ceramics was obtained using the material removal in the unit time as a bridge. Xiao et al. [15] proposed a theoretical model for ultrasonic vibration-assisted side grinding of ceramics with the consideration of the ductile-to-brittle transition removal mechanism and conducted experiments of zirconia ceramics to validate the proposed model which proved to be in good agreement with the experimental data. Zhang et al. [16] performed an experiment of ultrasonic assisted micro-end grinding for silica glass and Al_2O_3 ceramic, and results indicated that the micro-end grinding zone was divided into three grinding regions, namely, main grinding region, plowing grinding region, and sliding grinding region. Then, the grinding force model of the whole grinding wheel considering size effect was established. The foregoing researches have described the removal of materials under ultrasonic grinding in more detail, and the corresponding grinding force models have been established. However, these models mostly involve high hardness and low fracture toughness materials such as ceramic and carbon fiber composites, and research on high strength alloy steel remains rare. Since the removal methods for alloy steel and hard brittle materials such as ceramics are different, more in-depth studies are still required to investigate the effect of ultrasonic grinding on the removal of high strength alloy steel.

As a compound process, ultrasonic vibration will affect the grinding process at all times. Exploring the influence of ultrasonic vibration on the grinding process is of great significance for understanding the mechanism of ultrasonic grinding. Li et al. [17] conducted an experimental study on the ultrasonic vibration-assisted grinding of Inconel 718. The experimental results show that the ultrasonic vibration of the grinding wheel will reduce the length and cross-section area of the chips. The shear and flow of the chips will be reduced under large amplitudes, while they are little affected by the wheel speed. Tang et al. [18] mainly considered the influence of ultrasonic vibration on chip deformation force and friction force and established the grinding force model of ultrasonic grinding of 21NiCrMo5H. Cao et al. [19, 20] conducted the simulation and experimental research on the ultrasonic assisted grinding of single grain and found that the impact of the blade tip caused by ultrasonic vibration is the main factor to improve the cutting ability of the tool. Most studies have analyzed the influence of ultrasonic vibration on the grinding process through experimental phenomena or overall grinding force. The different states of grains in ultrasonic grinding process are not clearly stated. Therefore, a comprehensive and detailed description of the ultrasonic grinding force model for the ultrasonic grinding process is needed based on the ultrasonic grinding mechanism.

12Cr2Ni4A is a fine alloy structural steel, which not only has high yield strength, tensile strength, and fatigue strength but also has good plasticity, toughness, and high hardenability. It is mainly used to make various high-performance gears. With 12Cr2Ni4A alloy steel as the research object, a refined method for establishing a grinding force model of ultrasonic grinding of high strength alloy steel is proposed in this paper. The cutting process of the grains is divided into two stages, plowing stage and the chip forming stage. Meanwhile, considering the influence of ultrasonic vibration, the grinding force of each stage is modeled, and the interference between the trajectories of the abrasive grains caused by ultrasonic vibration is analyzed. Through the ultrasonic grinding experiment of 12Cr2Ni4A, the theoretical analysis and the correctness of the model are verified.

2 Kinematics analysis of single grain during UVAG

It is necessary to analyze the motion state of the grains and the workpiece for studying the mechanism of ultrasonic grinding. UVAG is composed of ultrasonic machining and grinding, as illustrated in Fig. 1. In ultrasonic grinding, there are three kinds of motion: the rotation movement of the grinding wheel, the feed movement of the workpiece, and the ultrasonic vibration along the axial direction of the grinding wheel.

Assuming that the abrasive grains are cones of the same size, and the grains are evenly distributed on the surface of the grinding wheel at the same grinding depth. With the point at which the grain begins to cut into the workpiece as the origin of coordinates, the three-dimensional coordinate system is established, as shown in Fig. 2. The grains cut into the workpiece from point B and cut out the workpiece from point F. The kinematic equation for the single grain in the three coordinate directions about motion time t can be expressed as

$$\begin{cases} x = v_w t + \dfrac{d_s}{2}\sin(2\pi n_s t) \\ y = \dfrac{d_s}{2}(1-\cos(2\pi n_s t)) \\ z = A\sin(2\pi f t) \end{cases} \tag{1}$$

In a grinding wheel rotation cycle, the cutting time can be expressed as

$$t_c = \frac{\sqrt{a_p d_s}}{v_s} \tag{2}$$

where v_w is work speed, n_s is grinding wheel speed, d_s is wheel diameter, a_p is grinding depth, A is ultrasonic amplitude, and f is ultrasonic frequency. In common grinding (CG), $A = 0$ and $f = 0$.

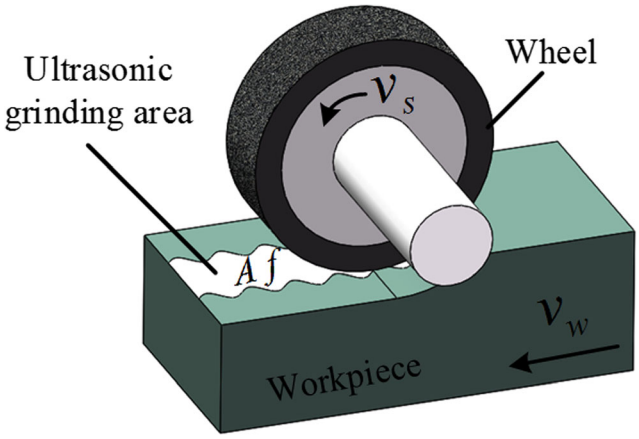

Fig. 1 Schematic diagram of UVAG

The velocity of the diamond grit in three coordinate directions can be obtained by differentiating Eq. (1), as shown in the following equation

$$\begin{cases} v_x = v_w + v_s\cos(2\pi n_s t) \\ v_y = v_s\sin(2\pi n_s t) \\ v_z = 2\pi A f\cos(2\pi f t) \end{cases} \tag{3}$$

The angle between the movement direction of the abrasive grain and the main cutting direction can be expressed as follows: $\phi_c = \tan^{-1}\left(\frac{2\pi A f\cos(2\pi f t)}{v_s}\right)$.

The chip thickness of the abrasive grain is an important factor affecting the grinding force and the mechanism of material removal. From the above analysis, it is known that the chip thickness of UVAG and CG at time t is $h(t)$. At this time, the rotation angle of the abrasive grain can be expressed as

$$\theta' = \frac{2\pi n_s}{60} t \tag{4}$$

$$\varphi = \frac{\pi}{2} + \theta' \tag{5}$$

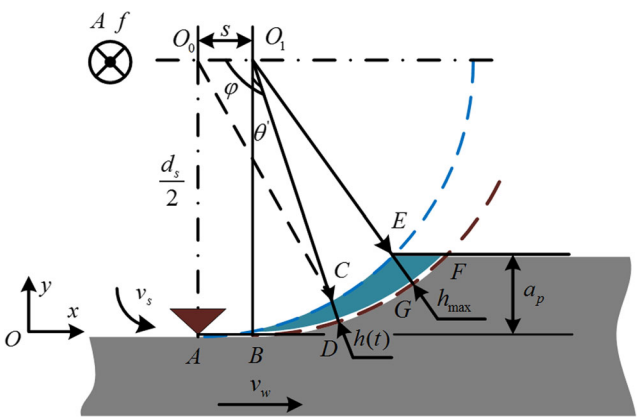

Fig. 2 Single grain trajectory in UVAG

The length of O_1Ccan be expressed as

$$O_1C = \frac{2s\cos(\varphi) + \sqrt{4s^2\cos^2(\varphi) - 4s^2 + {d_s}^2}}{2} \tag{6}$$

The chip thickness in UVAG can be expressed as

$$h(t) = \frac{d_s}{2} - \frac{2s\cos(\varphi) + \sqrt{4s^2\cos^2(\varphi) - 4s^2 + {d_s}^2}}{2} \tag{7}$$

where s is workpiece translation within adjacent intervals, $s = \frac{Lv_w}{v_s} + v_w t$, and L is the interval of two continuous cutting edges.

When $v_s = 10$ m/s, $v_w = 120$ mm/min, $a_p = 10$ μm, $A = 10$ μm, and $f = 20$ kHz ,the space position of the grain at every moment can be obtained as shown in Fig. 3. In UVAG, the grain cuts in and out of the x–O–y plane in the same way as in CG. In addition, the ultrasonic vibration makes the grain form a normal sine curve in the x–O–z plane.

3 Grain–workpiece contact and material removal rate

3.1 Grain–workpiece contact

In the grinding process, it is generally considered that abrasive grains go through three stages: sliding, plowing, and chip forming [21]. In the sliding stage, the material only takes elastic deformation, and the material returns to the initial state after the grains slide from the workpiece surface. In fact, for metal materials, plastic deformation has started when the abrasive grains begin to contact the materials. Jiang [22] used the Hertz contact theory to calculate the critical plowing thickness of the stage from the sliding stage to the plowing stage, and the critical value obtained is minimal. Therefore, this paper analyzes the contact between the abrasive grain and the workpiece under ultrasonic grinding, considering only the plowing stage and the chip forming stage.

In the plowing stage, as the cutting process proceeds, the chip thickness of the abrasive grain increases gradually, and the material is extruded with plastic deformation, thus forming a bulge on both sides of the grain, as shown in Fig.4a. In UVAG, the direction of the abrasive grain squeezing the workpiece is continually changing because of the effect of ultrasonic vibration. Therefore, the pileup formed on both sides of the abrasive grain is distinct from the symmetry featuring in the CG. The axis y_0 is the velocity direction of the abrasive grain in common grinding, the axis y_1 is the instantaneous velocity direction of the abrasive grain, and $\phi_c$is the angle between the abrasive grain velocity and the workpiece feeding direction. The dark part is the contact area between the abrasive grain and the material. Figure 4b is a projection of the *B*–*B* section of Fig 4a, and A_1 and A_2 are the uplift areas at the two sides of the abrasive grain at the maximum amplitude ($A_1 < A_2$).

As the cutting process proceeds further, when the abrasive grain reaches the critical chip thickness, the chip starts to peel off the workpiece, thus entering the chip forming stage until the

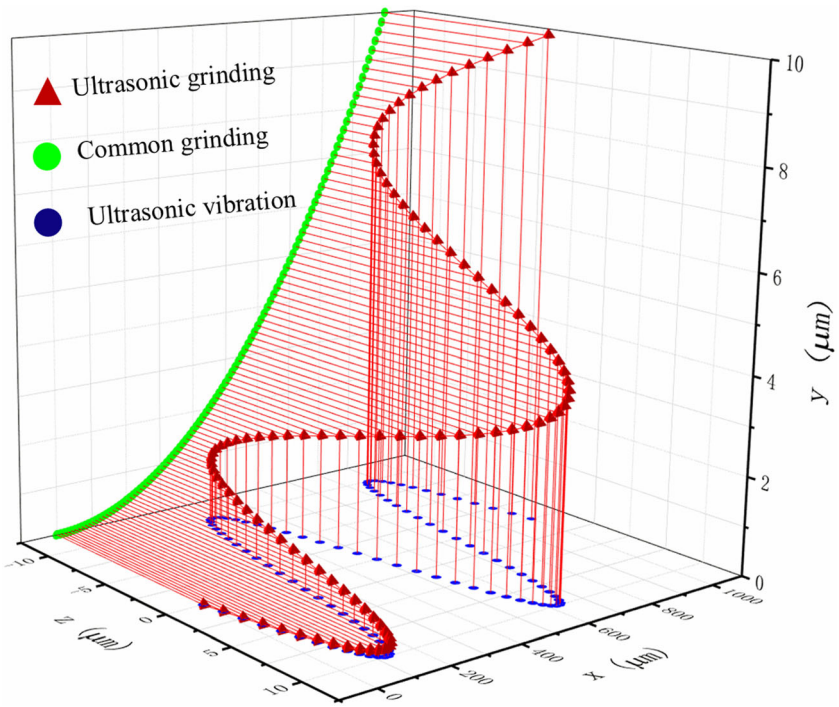

Fig. 3 Three-dimensional motion trajectory of single grain in UVAG

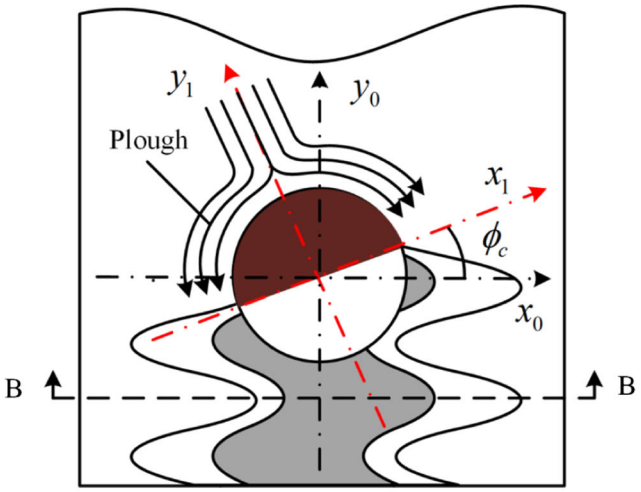

(a) Flow of material along edge of abrasive grain

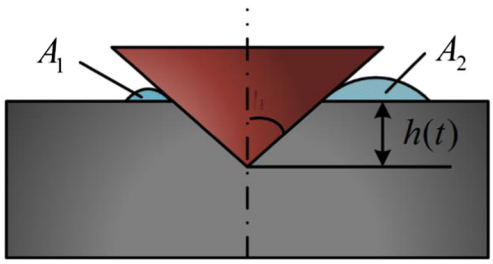

(b) Pileup of material on both sides of abrasive grain at the amplitude

Fig. 4 Plowing stage of single grain in UVAG. **a** Flow of material along edge of abrasive grain. **b** Pileup of material on both sides of abrasive grain at the amplitude

workpiece surface is cut out. This ends the cutting process of the abrasive grain in a grinding wheel rotation cycle, as shown in Fig. 5.

3.2 Material removal rate of ultrasonic grinding with single abrasive grain

Equation (7) is the function of chip thickness versus time t. The abrasive grain enters the plowing stage from the moment 0 and enters the chip forming stage at t_p. The chip thickness at the moment t_p is the critical chip thickness of the abrasive grain, as shown in Fig. 6. As investigated in previous research [23], $h(t_p) = 0.05r_g$ in dry grinding, where r_g is radius of cutting edge. The plowing length of the abrasive grain l_p can be expressed as

$$l_p = \int_0^{t_p} \left[(v_w + v_s \cos(2\pi n_s t))^2 + (v_s \sin(2\pi n_s t))^2 + (2\pi A f \cos(2\pi f t))^2 \right]^{\frac{1}{2}} dt \quad (8)$$

The cutting length from time $t_p$to time t_c is the length of the chip formation which can be expressed as

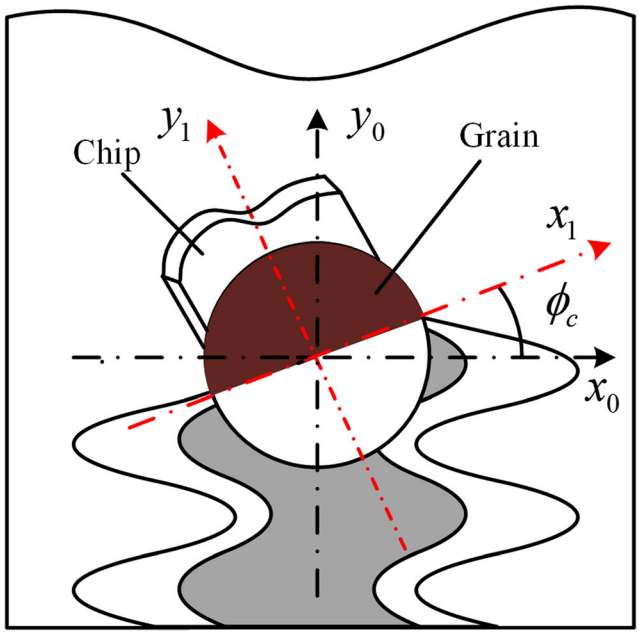

Fig. 5 Chip forming stage of single grain in UVAG

$$l_c = \int_{t_c}^{t_p} \left[(v_w + v_s \cos(2\pi n_s t))^2 + (v_s \sin(2\pi n_s t))^2 + (2\pi A f \cos(2\pi f t))^2 \right]^{\frac{1}{2}} \quad (9)$$

The abrasive grains squeeze the workpiece during the plowing stage, and the material produces the plowing flow to both sides of the abrasive grain, but the material is not removed. Therefore, the abrasive grain only removes the material during the chip forming stage. The actual volume of material removed by a single abrasive grain during a cutting process can be expressed as

$$V_{uc} = \int_{t_c}^{t_p} h(t)^2 \tan(\gamma_0) \left[(v_w + v_s \cos(2\pi n_s t))^2 + (v_s \sin(2\pi n_s t))^2 + (2\pi A f \cos(2\pi f t))^2 \right]^{\frac{1}{2}} \quad (10)$$

Therefore, the actual material removal rate of single abrasive grain in UVAG can be expressed as

$$SMRR = \frac{V_{uc}}{t_c - t_p} \quad (11)$$

4 Procedure of modeling cutting force during UVAG

4.1 Grinding force during plowing stage

When $h(t) < h(t_p)$, the material is extruded and accumulated on both sides of the abrasive grain. Instantaneous chip thickness has not reached the condition of chip formation, so the abrasive grain is in the plowing stage. The force acting on the contact surface of the abrasive grain is shown in Fig. 7a.

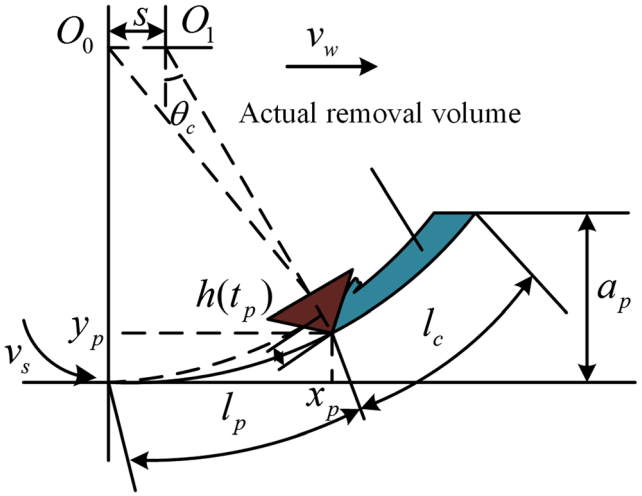

Fig. 6 Two stages of abrasive grain cutting for material removal

Since the material flows along the side of the abrasive grain to the two sides, the friction force experienced by the abrasive grain in the plowing stage is opposite to the flow direction of the material, as shown in Fig. 7b.

The plowing force perpendicular to the contact surface of the abrasive grain is the product of the yield stress of the material and the contact area

$$\mathrm{d}F_{l-np} = \delta_p dA_p \tag{12}$$

where δ_p is the yield stress of the material.

The friction force can be expressed as

$$\mathrm{d}F_{l-fp} = \mu_p \mathrm{d}F_{l-np} \tag{13}$$

where μ_p is the friction coefficient between the grain and the workpiece during the plowing stage. According to [24], $\mu_p = \frac{2}{\pi}\cot\gamma_0$.

Unit contact area can be calculated by

$$dA_p = \frac{1}{2}h(t)^2\frac{\tan(\gamma_0)}{\cos(\gamma_0)}d\alpha \tag{14}$$

The differential equations of plowing force in normal and tangential directions can be derived as

$$\mathrm{d}F_{npy} = \delta_p dA_p \sin\gamma_0 \tag{15}$$

$$\mathrm{d}F_{npx} = \delta_p dA_p \cos\gamma_0 \cos\alpha \cos\phi_c \tag{16}$$

The differential equation of friction force can be derived as

$$\mathrm{d}F_{fpx} = \mu_p \delta_p dA_p \cos\alpha \cos\phi_c \tag{17}$$

Therefore, the integral of the plowing force in the contact area of the abrasive grain and the workpiece can be obtained as

$$\begin{aligned} F_{py} &= 2\int_0^{\frac{\pi}{2}} \frac{1}{2}\delta_p h(t)^2 \frac{\tan(\gamma_0)}{\cos(\gamma_0)}\sin\gamma_0 d\alpha \\ &= \frac{\pi}{2}\delta_p h(t)^2 \tan^2(\gamma_0) \end{aligned} \tag{18}$$

The tangential plowing force integral of the workpiece feed direction can be obtained as

$$\begin{aligned} F_{px} &= 2\int_0^{\frac{\pi}{2}} \frac{1}{2}\delta_p h(t)^2 \tan(\gamma_0)\cos\alpha\cos\phi_c d\alpha + \frac{1}{2}\mu_p\delta_p h(t)^2\frac{\tan(\gamma_0)}{\cos(\gamma_0)}\cos\alpha\cos\phi_c d\alpha \\ &= \delta_p h(t)^2 \frac{\tan(\gamma_0)}{\cos(\gamma_0)}\left(\cos\gamma_0 + \mu_p\right)\cos\phi_c \end{aligned} \tag{19}$$

4.2 Grinding force during chip forming stage

When $h(t) > h(t_p)$, the abrasive grain shears the material, and a chip along the contact surface between the abrasive grain and the workpiece is formed, as shown in Fig 8a. The force acting on the contact surface of the chip and the abrasive grain at this time includes the normal force $F_n$and the friction force $F_f$along the contact surface. F_r is the combined force of normal force and friction force, and the angle of friction β is between F_n and F_f. The normal force F_{ns} and shear force F_s act on the shear surface. The shear angle ϕ is the angle between the shear force and the cutting direction of the abrasive grain. The force on the contact surface is balanced with force on the shear surface, as illustrated in Fig. 8b.

The differential equations of the cutting area A_D and the sectional area $A_S$of the shear plane can be expressed as

$$\mathrm{d}A_D = h(t)^2 \tan\gamma_0 \mathrm{d}\varphi \tag{20}$$

$$\mathrm{d}A_S = \frac{\mathrm{d}A_D}{\sin\phi} = \frac{h(t)^2\tan\gamma_0 \mathrm{d}\varphi}{\sin\phi} \tag{21}$$

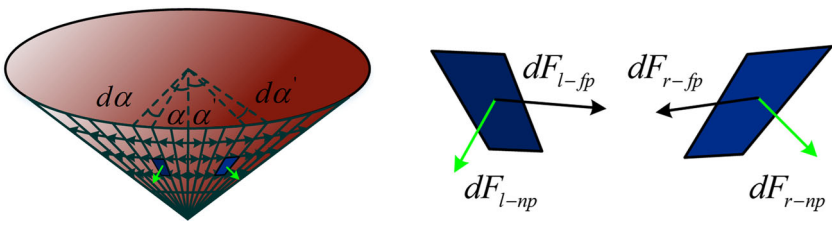

(a) Abrasive grain contact surface (b) Abrasive grain-workpiece contact force

Fig. 7 Grinding force during plowing stage. **a** Abrasive grain contact surface. **b** Abrasive grain–workpiece contact force

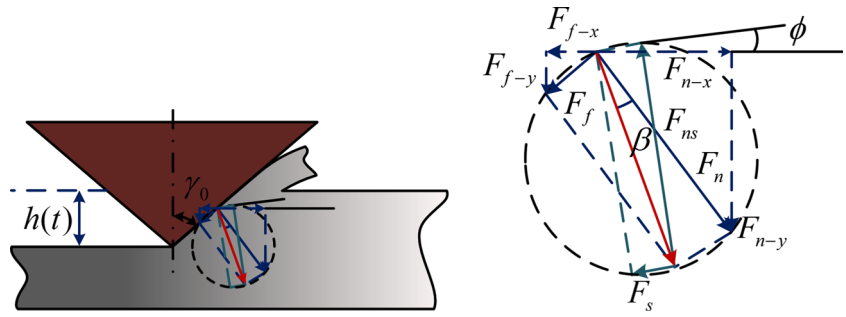

(a) Chip forming of abrasive grain (b) Abrasive grain and contact surface force

Fig. 8 Grinding force at chip forming stage. **a** Chip forming of abrasive grain. **b** Abrasive grain and contact surface force

The shear force on the unit area can be derived as

$$\mathrm{d}F_s = \tau_s \mathrm{d}A_S = \frac{\tau_s h(t)^2 \tan\gamma_0 \mathrm{d}\varphi}{\sin\phi} \tag{22}$$

where $\tau_s$is the shear stress on the shear surface.

The combined force of normal force and friction force on the unit area can be derived as

$$\mathrm{d}F_r = \frac{\tau_s h(t)^2 \tan\gamma_0 \mathrm{d}\varphi}{\sin\phi\cos(\phi+\beta+\gamma_0)} \tag{23}$$

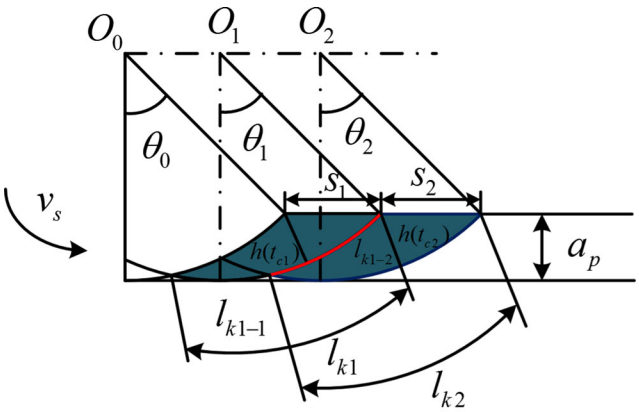

(a) Adjacent abrasive grain trajectory in normal interference

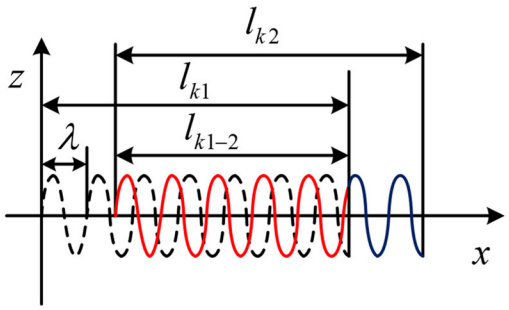

(b) Adjacent abrasive grain trajectory in axial interference

Fig. 9 Adjacent abrasive grain trajectory interference. **a** Adjacent abrasive grain trajectory in normal interference. **b** Adjacent abrasive grain trajectory in axial interference

Then, the normal force of the unit area in the y-direction can be derived as

$$\begin{aligned}\mathrm{d}F_{r-y} &= \mathrm{d}F_r\cos\beta\sin\gamma_0 + \mathrm{d}F_r\sin\beta\cos\gamma_0 \\ &= \frac{\tau_s h(t)^2\tan\gamma_0}{\sin\phi\cos(\phi+\beta+\gamma_0)}\sin(\beta+\gamma_0)\mathrm{d}\varphi\end{aligned} \tag{24}$$

The tangential force of the unit area in the x-direction can be derived as

$$\begin{aligned}\mathrm{d}F_{r-x} &= (\mathrm{d}F_r\cos\beta\cos\gamma_0 - \mathrm{d}F_r\sin\beta\sin\gamma_0)\cos\varphi \\ &= \mathrm{d}F_r\cos(\beta+\gamma_0)\cos\varphi\end{aligned} \tag{25}$$

Therefore, the normal force in the contact zone in UVAG can be expressed as

$$\begin{aligned}F_{cy} &= \int_0^{\pi}\frac{\tau_s h(t)^2\tan\gamma_0}{\sin\phi\cos(\phi+\beta+\gamma_0)}\sin(\beta+\gamma_0)\mathrm{d}\varphi \\ &= \frac{\pi\tau_s h(t)^2\tan\gamma_0}{\sin\phi\cos(\phi+\beta+\gamma_0)}\sin(\beta+\gamma_0)\end{aligned} \tag{26}$$

The tangential force in the contact zone in UVAG can be expressed as

$$\begin{aligned}F_{cx} &= \int_0^{\pi}\frac{\tau_s h(t)^2\tan\gamma_0}{\sin\phi\cos(\phi+\beta+\gamma_0)}\cos(\beta+\gamma_0)\sin\varphi\mathrm{d}\varphi\cos\phi_c \\ &= \frac{2\tau_s h(t)^2\tan\gamma_0}{\sin\phi\cos(\phi+\beta+\gamma_0)}\cos(\beta+\gamma_0)\cos\phi_c\end{aligned} \tag{27}$$

According to [25], shear angle ϕ can be obtained as $\phi = \frac{\pi}{4} - \frac{\beta-\gamma_0}{4}$.

The friction angle β can be obtained by the friction coefficient between the abrasive grain and the chip. Their relationship can be expressed as

$$\mu_c = \tan\beta \tag{28}$$

5 Interference of grain trajectory in UVAG

The grinding process is the result of multiple abrasive grains cutting the material together. Due to the axial ultrasonic vibration, the mutual interference between the abrasive trajectories is more complicated, and the greatest influence is the interference between adjacent abrasive grains. Since the amplitude of the ultrasonic vibration applied in the axial direction of the grinding wheel is usually 5–25 μm, which is much smaller than the distance between the axial abrasive grains of the grinding wheel, there is little interference between the abrasive grains. Therefore, only the two adjacent abrasive grains on the circumference of the grinding wheel are analyzed here. The interaction between the abrasive grains on the circumference of the grinding wheel is mainly composed of two aspects in UVAG. On the one hand, at the feed direction, an abrasive grain continues to cut the material on the cutting surface of the previous abrasive grain, as shown in Fig. 9a. On the other hand, two adjacent abrasive grains interfere with each other on the cutting trajectory in the axial direction, as shown in Fig. 9b. The distance traveled by the abrasive grain during a vibration cycle is one wavelength which can be expressed as

$$\lambda = \frac{v_s + v_w}{f} \tag{29}$$

The cutting arc length of the preceding abrasive grain in the axial direction of the grinding wheel can be derived as

$$l_{k1} = l_{k1-1} + l_{k1-2} \tag{30}$$

Then, the interference length of the abrasive grain trajectory before and after the grinding wheel can be deduced as

$$l_{k1-2} = \sqrt{\left(l_{k2} - \sqrt{{s_2}^2 - h(t_{c2})^2}\right)^2 + h(t_{c2})^2} \tag{31}$$

where $h(t_{c1})$ and $h(t_{c2})$ are the maximum chip thickness of the first and second abrasive grains, respectively.

The number of interference vibration periods of two adjacent abrasive grain trajectories in the axial direction of the grinding wheel can be obtained as

$$n = \frac{l_{k1-2}}{\lambda} \tag{32}$$

For each vibration cycle, the trajectory of the abrasive grain interferes twice, and the number of trajectory interferences can be expressed as

$$m = 2n \tag{33}$$

From the above analysis, it can be observed that the number of interferences of the abrasive grain trajectory is related to the parameters of the wheel and the grinding conditions. In fact, the interferences between the abrasive grains turn the process of material removal from the workpiece into intermittent cutting. The empty cutting contributes to grinding force reduction, accelerates the cooling of the grinding heat and makes it easier for the material to form swarf. Therefore, it is possible to increase the interference of abrasive grain trajectory in a certain range to improve the grinding quality.

6 Grinding force model in ultrasonic grinding zone

6.1 Number of active abrasive grains involved in grinding

The number of active abrasive grains in the grinding zone is an important factor affecting the ultrasonic grinding force in the grinding zone under different machining parameters. Studies have shown that the number of active abrasive grains is little affected by wheel speed and workpiece feed rate but significantly influenced by grinding depth [26]. The greater the grinding depth is, the more abrasive grains will participate in the grinding. From Setti's [27] results, at a certain grinding depth, the probability of abrasive grains participating in grinding on the grinding wheel is shown in Eq. (34).

$$P(N_s) = P\left(X \geq d_{\mathrm{gc}}\right) = P\left(Z \geq \left(\frac{d_{\mathrm{gc}} - \mu_g}{\sigma}\right)\right) \tag{34}$$

where $d_{\mathrm{gc}} = d_{\mathrm{gmax}} - a_p$, $\mu_g = d_{\mathrm{gmean}}$ and $\sigma = \frac{d_{\mathrm{gmax}} - d_{\mathrm{gmean}}}{3}$.

The number of abrasive grains participating in ultrasonic grinding in the plowing zone can be expressed as

$$N_p = P(N_s) N_a l_p b = P(N_s) N_a b \Big|_0^{t_p} \left[\left(v_w + v_s \cos(2\pi n_s t)\right)^2 + \left(v_s \sin(2\pi n_s t)\right)^2 + \left(2\pi A f \cos(2\pi f t)\right)^2\right]^{\frac{1}{2}} dt \tag{35}$$

The number of abrasive grains participating in ultrasonic grinding in the chip forming zone can be expressed as

$$N_c = P(N_s) N_a l_c b = P(N_s) N_a b \Big|_{t_p}^{t_c} \left[\left(v_w + v_s \cos(2\pi n_s t)\right)^2 + \left(v_s \sin(2\pi n_s t)\right)^2 + \left(2\pi A f \cos(2\pi f t)\right)^2\right]^{\frac{1}{2}} dt \tag{36}$$

where b is grinding width, l_p and l_c are determined by Eqs. (8) and (9), and N_a is the number of abrasive grains per unit area of the surface of the grinding wheel which can be measured by experiment.

6.2 Ultrasonic grinding force model

In the actual ultrasonic grinding process, there are influences that cannot be accurately determined for the grinding force models.

Firstly, the abrasive grains are assumed to be cones in Section 1 to simplify the analysis. As a matter of fact, the shape of the abrasive grains is random. The simplification will produce deviation to the calculation of grinding force. Secondly, with the progress of the grinding process, the grinding force will be affected by the breakage, falling, and abrasion wear of grinding particles on the grinding wheel under different processing parameters. Thirdly, the analysis in Section 4 reveals that the trajectories between abrasive grains will cause interference in the actual grinding process to generate empty cutting, and the addition of ultrasonic vibration will increase this interference effect and further affect the grinding force. These factors are related to grinding depth a_p, grinding speed v_s, and ultrasonic amplitude A, and their influence on the grinding force will always present throughout the entire ultrasonic grinding process. In this paper, the parameter $K = k{a_p}^{a_1}{v_s}^{a_2}A^{a_3}$ is introduced to incorporate the ultrasonic effect into the grinding force model, where k, a_1, a_2, and a_3 represent the influence of model simplification, the depth of the grinding, the grinding speed, and the ultrasonic amplitude on the grinding force in the parameter K respectively.

Therefore, the normal grinding force in the ultrasonic grinding zone can be expressed as

$$F_n = K\left(\sum_1^{N_p} F_{py} + \sum_1^{N_c} F_{cy}\right) = \mathrm{K}\sum_1^{N_p}\frac{\pi}{2}\delta_p h(t)^2\tan^2(\gamma_0) + \mathrm{K}\sum_1^{N_c}\frac{\pi\tau_s h(t)^2\tan\gamma_0}{\sin\phi\cos(\phi+\beta+\gamma_0)}\sin(\beta+\gamma_0) \quad (37)$$

The tangential grinding force in the ultrasonic grinding zone can be expressed as

$$\begin{aligned} F_t &= K\left(\sum_1^{N_p} F_{px} + \sum_1^{N_c} F_{cx}\right) \\ &= K\sum_1^{N_p}\delta_p h(t)^2\frac{\tan\gamma_0}{\cos\gamma_0}\left(\cos\gamma_0 + \mu_p\right)\cos\phi_c \\ &\quad + \mathrm{K}\sum_1^{N_c}\frac{2\tau_s h(t)^2\tan\gamma_0}{\sin\phi\cos(\phi+\beta+\gamma_0)}\cos(\beta+\gamma_0) \end{aligned} \quad (38)$$

Equations (37) and (38) are the ultrasonic normal and tangential grinding force models for alloy structural steel. The K value in the formula is determined by the experiment, $h(t)$ is chip thickness which can be determined by Eq. (7), and $N_p$and N_c can be determined by Eqs. (35) and (36). The remaining parameters are determined by the grinding wheel parameters, workpiece parameters, or machining parameters.

7 Experiment verification

7.1 Experimental details

To deeply explore the mechanism of ultrasonic grinding, obtain the accurate model of the ultrasonic grinding force of high-strength alloy steel, and verify the proposed model, the ultrasonic grinding test bench was

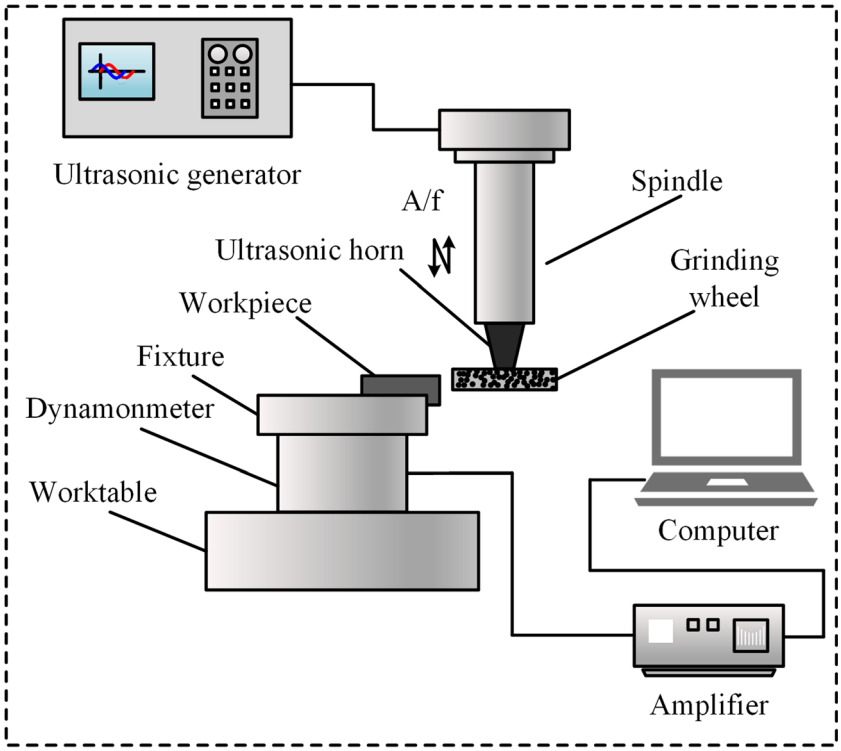

Fig. 10 Schematic diagram of ultrasonic grinding experiment system

set up and a series of ultrasonic grinding experiments were conducted, as shown in Fig. 10. The ultrasonic grinding equipment mainly includes an ultrasonic spindle system, a workpiece feed system, and a grinding force measurement system. The ultrasonic vibration system consists of an ultrasonic generator, a transducer, and a horn. The ultrasonic power is controlled by adjusting the ultrasonic generator. The ultrasonic vibration device is connected to the spindle of the machine tool, and ultrasonic vibration is added along the axis of the grinding wheel.

The ultrasonic generator can automatically track the resonant frequency of the ultrasonic vibration system and output the frequency value on the display screen. The ultrasonic frequency measured in this experiment is 25 kHz. The vibration amplitudes of the grinding wheel in the axial direction were measured using a laser displacement sensor (LK-G10 by KEYENCE). In this paper, ultrasonic grinding with 20%, 30%, and 40% ultrasonic power is carried out. The measured amplitudes are approximately proportional to the ultrasonic power, which are 4 μm, 7 μm, and 10 μm, respectively.

The grinding wheel is a resin type CBN grinding wheel, and the workpiece material is 12Cr2Ni4A. The grinding force is measured in real time by a three-dimensional dynamometer (9257B) with a sampling frequency of 30 kHz. The values of grinding wheel parameters, workpiece parameters, grinding parameters, and ultrasonic parameters are shown in Table 1. Each group was repeated three times to reduce the experimental random error.

7.2 Experimental results and discussion

When the spindle rotation speed is 1500 r/min, and the grinding depth is 5–30 μm, the change of normal and tangential grinding forces with ultrasonic amplitude is shown in Fig. 11. When the ultrasonic amplitude is zero, it is common grinding. It can be seen from the diagram that both the normal grinding force and the tangential grinding force increase with the grinding depth. The growth of the grinding depth not only increases the number of active abrasive grains per unit area but also increases the cutting length and the chip thickness, which leads to an increase in the grinding force. With the rise of ultrasonic amplitude, the grinding force is decreasing at every grinding depth, which indicates that the addition of ultrasonic vibration is helpful to reduce the grinding force, and the effect of ultrasonic vibration on the grinding force is not influenced by different grinding depths. The reason is that the increase of ultrasonic amplitude strengthens the interference and repeated cutting effect of the intergranular cutting trajectory, while the grinding depth has little influence on the interference of the abrasive trajectory.

As shown in Fig. 12, the grinding force decreases with the increase of grinding wheel speed. This is mainly because the increase of the grinding wheel speed decreases the average chip thickness, and the number of grinding grains involved in grinding is not changed, which leads to the decrease of the grinding force. As the speed of the grinding wheel increases, the effect of ultrasonic vibration on the grinding force decreases gradually. When the spindle rotation speed is 3000 r/min, it almost does not affect the grinding force. Therefore, the

Table 1 Experimental parameters

Type	Parameters	Value
Wheel parameters	Grinding wheel	CBN #120
	Grinding wheel size (mm)	$d_s = 100$
	Number of grits per unit area	$N_a = 22.595$
	Maximum grain diameter (mm)	$d_{\mathrm{gmax}} = 0.139$
	Minimum grain diameter (mm)	$d_{\mathrm{gmin}} = 0.114$
Workpiece parameters	Workpiece size (mm)	$16 \times 9 \times 9$
	Density (g/cm^3)	$\rho = 7.84$
	Young's modulus (Gpa)	$E = 211$
	Poisson ratio	$\nu = 0.29$
	Yield strength (Mpa)	$\sigma_p = 785$
	Shear strength (Mpa)	$\tau = 552$
Grinding parameters	Coolant	Without
	Grinding depth (μm)	$a_p = 5, 10, 15, 20, 25, 30$
	Spindle rotation speed (r/min)	$n_s = 500, 1000, 1500, 2000, 2500, 3000$
	Worktable feed rate (mm/min)	$v_w = 300$
Ultrasonic parameters	Ultrasonic amplitude (μm)	$A = 0, 4, 7, 10$
	Ultrasonic frequency (kHz)	$f = 25$

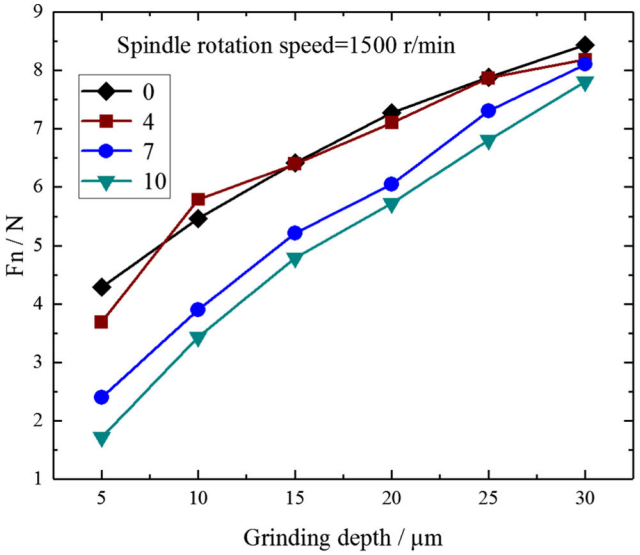

(a) Normal grinding force

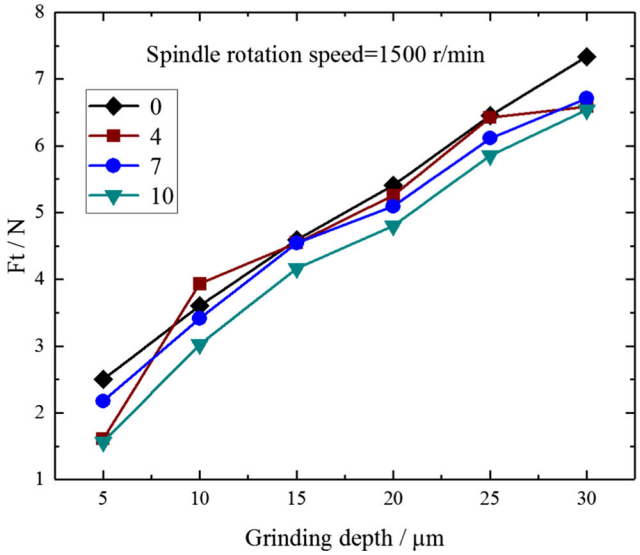

(b) Tangential grinding force

Fig. 11 Relation between grinding force and grinding depth under different ultrasonic amplitudes. **a** Normal grinding force. **b** Tangential grinding force

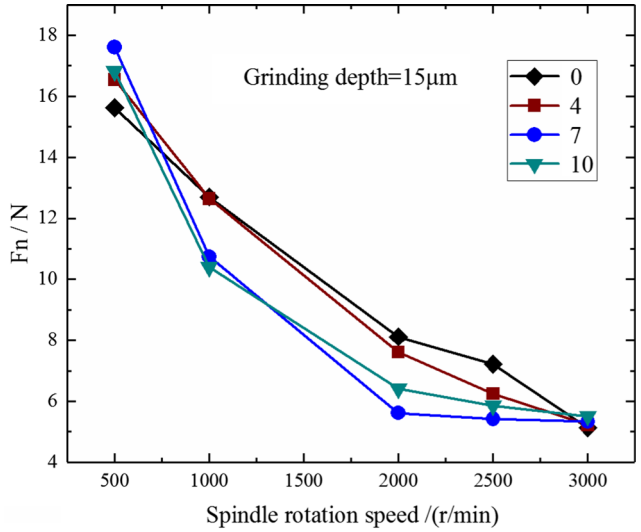

(a) Normal grinding force

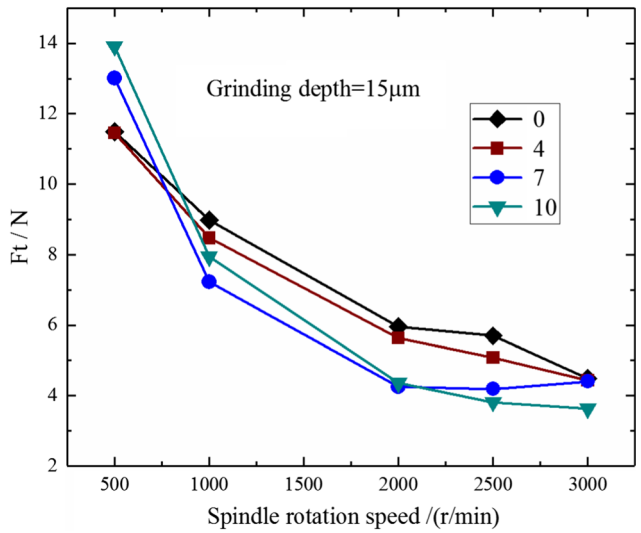

(b) Tangential grinding force

Fig. 12 Relation between grinding force and spindle rotation speed under different ultrasonic amplitudes. **a** Normal grinding force. **b** Tangential grinding force

application of UVAG to reduce the grinding force should be controlled under the appropriate processing parameters.

7.3 Determination of parameter *K* and validation of the model

The grinding force data obtained from the ultrasonic grinding experiment mentioned in Section 7.1 to verify the model of ultrasonic grinding force and determine the parameter K. Each variable was taken at several levels while keeping other variables constant. The parameter K (k, a_1, a_2, a_3) can be deduced through nonlinear curve fitting. It can be expressed as $K = 5.13 \times 10^{-5} \cdot {a_p}^{-0.4252} \cdot {v_s}^{0.4469} \cdot A^{-0.6591}$.

The grinding parameters in the experiment are substituted into the theoretical model to obtain the grinding force values of the experiment and the model under different parameters. The calculated results of the normal and tangential forces are compared with the experimental data as shown in Fig. 13. The grinding force increases with the increase of grinding depth, while it decreases with the increase of spindle rotation speed and ultrasonic amplitude. The trends of the predicted grinding forces are in good agreement with the measured. The average percentage of the deviation in the normal grinding force is 8.04%, while the average percentage of the deviation in the tangential grinding force is 10.06%. There are two main

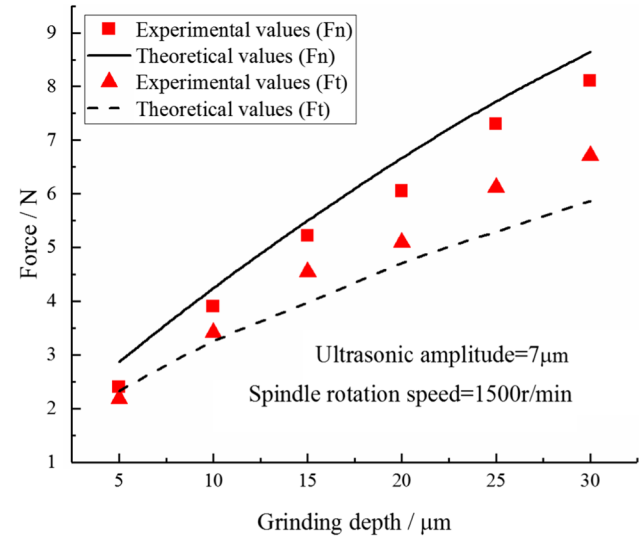

(a) Grinding depth

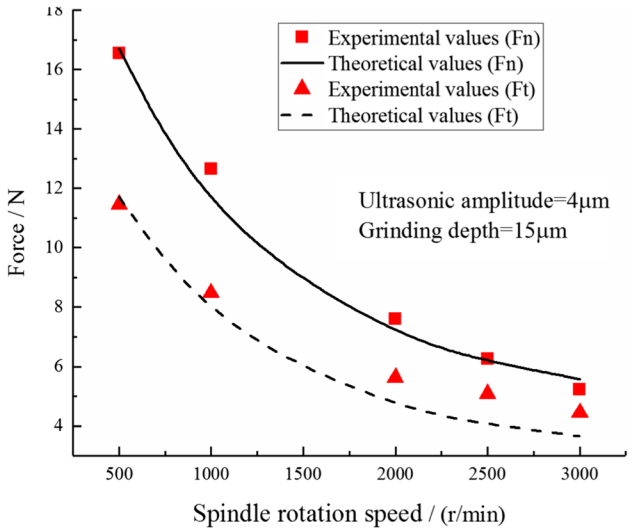

(b) Spindle rotation speed

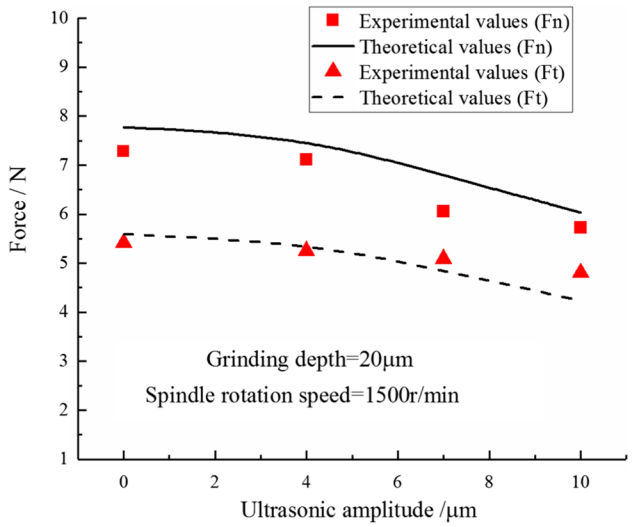

(c) Ultrasonic amplitude

◀ **Fig. 13** Comparison of grinding force between theoretical values and experimental values. **a** Grinding depth. **b** Spindle rotation speed. **c** Ultrasonic amplitude

reasons might account for these in the ultrasonic grinding tests. On one hand, the slight radial vibration caused by the axial ultrasonic vibration influences the grinding force in the performed experiments. On the other hand, machine tools inevitably generate transmission errors and vibrations in the actual grinding process, which leads to errors in model results and experimental results.

The model is based on the chip thickness of the abrasive grains and covers the state of the force at each stage of the grinding process. The thickness of the abrasive grain, the number of grains involved in grinding, and the interference between the abrasive grains are essential factors that affect the grinding force. The addition of ultrasonic vibration has an important influence in these aspects. Compared with CG, ultrasonic vibration reduces the chip thickness of the abrasive grains and expands the area of the grinding zone, which increases the number of grains involved in grinding and raises the interference degree of the intergranular cutting trajectory. The influences of ultrasonic vibration on these parameters are reflected in the proposed model. Compared with the existing models, the factors that affect the ultrasonic grinding force are analyzed more comprehensively.

8 Conclusions

Based on the mechanism of ultrasonic grinding material removal, the ultrasonic grinding force calculation model of alloy structural steel 12Cr2Ni4A is established, and the ultrasonic grinding experiment is carried out to verify the model. The main conclusions are summarized as follows:

1. The calculation model of ultrasonic grinding force has taken into account the influence of plowing, friction, chip, ultrasonic vibration, abrasive grain trajectory interference, and the number of active abrasive grains. The material removal mechanism and contact state in ultrasonic grinding can be described in a more accurate and comprehensive way.
2. The calculation model of ultrasonic grinding force is proposed to predict the relationship between the grinding parameters, ultrasonic parameters, and grinding force. The grinding force increases with the grinding depth and decreases with the grinding wheel speed and ultrasonic amplitude. The ultrasonic vibration is helpful to reduce the grinding force, but it does not change the influence trend of grinding parameters on the grinding force.
3. The grinding force calculated by the ultrasonic grinding force model is consistent with the experimental trend with

the average deviations of the normal grinding force and the tangential grinding force being 8.04% and 10.06%, respectively.

The modeling method proposed in this paper provides a better understanding of the mechanism of UVAG. It not only establishes a comprehensive and detailed ultrasonic grinding force model of metal but also has great significance for the study of grinding heat and surface topography in ultrasonic machining.

Funding information The authors gratefully acknowledge the support of the National Natural Science Foundation of China (NSFC) through Grant Nos. 51535012, 51705542, and U1604255, the support of the Key Research and Development Project of Hunan province through Grant No. 2016JC2001, and the Fundamental Research Funds for the Central Universities of Central South University No. 2018zzts461.

References

1. Dambatta YS, Sarhan AAD, Sayuti M, Hamdi M (2017) Ultrasonic assisted grinding of advanced materials for biomedical and aerospace applications—a review. Int J Adv Manuf Technol 92(9–12): 3825–3858. https://doi.org/10.1007/s00170-017-0316-z
2. Chen HF, Tang JY, Zhou W (2013) An experimental study of the effects of ultrasonic vibration on grinding; surface roughness of C45 carbon steel. Int J Adv Manuf Technol 68(9–12):2095–2098. https://doi.org/10.1007/s00170-013-4824-1
3. Ding K, Fu YC, Su HH, Cui FF, Li QL, Lei WN, Xu HX (2017) Study on surface/subsurface breakage in ultrasonic assisted grinding of C/SiC composites. Int J Adv Manuf Technol 91(9–12):3095–3105
4. Ding K, Fu YC, Su HH, Xu HX, Cui FF, Li QL (2017) Experimental studies on matching performance of grinding and vibration parameters in ultrasonic assisted grinding of SiC ceramics. Int J Adv Manuf Technol 88(9–12):2527–2535
5. Shen JY, Wang JQ, Jiang B, Xu XP (2015) Study on wear of diamond wheel in ultrasonic vibration-assisted grinding ceramic. Wear 332-333: 788–793. https://doi.org/10.1016/j.wear.2015.02.047
6. Tawakoli T, Azarhoushang B (2008) Influence of ultrasonic vibrations on dry grinding of soft steel. Int J Mach Tools Manuf 48(14): 1585–1591
7. Tawakoli T, Azarhoushang B, Rabiey M (2008) Ultrasonic assisted dry grinding of 42CrMo4. Int J Adv Manuf Technol 42(9–10):883–891. https://doi.org/10.1007/s00170-008-1646-7
8. Wang Y, Lin B, Cao X, Wang S (2014) An experimental investigation of system matching in ultrasonic vibration assisted grinding for titanium. J Mater Process Technol 214(9):1871–1878. https://doi.org/10.1016/j.jmatprotec.2014.04.001
9. Rowe W (2009) Principles of modern grinding technology. William Andrew, Burlington
10. Liu D, Cong WL, Pei ZJ, Tang Y (2012) A cutting force model for rotary ultrasonic machining of brittle materials. Int J Adv Manuf Technol 52(1):77–84. https://doi.org/10.1016/j.ijmachtools.2011.09.006
11. Wang Y, Lin B, Wang S, Cao X (2014) Study on the system matching of ultrasonic vibration assisted grinding for hard and brittle materials processing. Int J Mach Tools Manuf 77:66–73. https://doi.org/10.1016/j.ijmachtools.2013.11.003
12. Ning F, Cong W, Wang H, Hu Y, Hu Z, Pei Z (2017) Surface grinding of CFRP composites with rotary ultrasonic machining: a mechanistic model on cutting force in the feed direction. Int J Adv Manuf Technol 92(1–4):1217–1229. https://doi.org/10.1007/s00170-017-0149-9
13. Cong WL, Pei ZJ, Sun X, Zhang CL (2014) Rotary ultrasonic machining of CFRP: a mechanistic predictive model for cutting force. Ultrasonics 54(2):663–675. https://doi.org/10.1016/j.ultras.2013.09.005
14. Li C, Zhang F, Meng B, Liu L, Rao X (2017) Material removal mechanism and grinding force modelling of ultrasonic vibration assisted grinding for SiC ceramics. Ceram Int 43(3):2981–2993. https://doi.org/10.1016/j.ceramint.2016.11.066
15. Xiao X, Zheng K, Liao W, Meng H (2016) Study on cutting force model in ultrasonic vibration assisted side grinding of zirconia ceramics. Int J Mach Tools Manuf 104:58–67. https://doi.org/10.1016/j.ijmachtools.2016.01.004
16. Zhang JH, Li H, Zhang ML, Zhao Y, Wang LY (2017) Study on force modeling considering size effect in ultrasonic-assisted micro-end grinding of silica glass and Al2O3 ceramic. Int J Adv Manuf Technol 89(1–4):1173–1192. https://doi.org/10.1007/s00170-016-9148-5
17. Li S, Wu Y, Nomura M (2016) Effect of grinding wheel ultrasonic vibration on chip formation in surface grinding of Inconel 718. Int J Adv Manuf Technol 86(1–4):1113–1125. https://doi.org/10.1007/s00170-015-8149-0
18. Tang J (2016) Modeling on grinding force assisted with axial ultrasonic vibration. Chin J Mech Eng 52(15):184. https://doi.org/10.3901/jme.2016.15.184
19. Cao J, Wu Y, Li J, Zhang Q (2015) Study on the material removal process in ultrasonic-assisted grinding of SiC ceramics using smooth particle hydrodynamic (SPH) method. Int J Adv Manuf Technol 83(5–8):985–994. https://doi.org/10.1007/s00170-015-7629-6
20. Cao J, Wu Y, Lu D, Fujimoto M, Nomura M (2014) Material removal behavior in ultrasonic-assisted scratching of SiC ceramics with a single diamond tool. Int J Mach Tools Manuf 79:49–61. https://doi.org/10.1016/j.ijmachtools.2014.02.002
21. Malkin S (1989) Grinding technology: theory and application of machining with abrasives. Ellis Harwood Publication, UK
22. Jiang J, Ge P, Sun S, Wang D, Wang Y, Yang Y (2016) From the microscopic interaction mechanism to the grinding temperature field: an integrated modelling on the grinding process. Int J Mach Tools Manuf 110:27–42. https://doi.org/10.1016/j.ijmachtools.2016.08.004
23. Hou ZB, Komanduri R (2003) On the mechanics of the grinding process—part I. Stochastic nature of the grinding process. Int J Mach Tools Manuf 43(15):1579–1593. https://doi.org/10.1016/s0890-6955(03)00186-x
24. Halling J (1975), Principles of tribology, Macmillan, London https://link.springer.com/book/10.1007%2F978-1-349-04138-1 [Accessed: 16-Nov-2018]
25. Merchant ME (1945) Mechanics of the metal cutting process. I. Orthogonal cutting and a type 2 chip. J Appl Phys 16(5):267–275
26. Zhang Y, Li C, Ji H, Yang X, Yang M, Jia D, Zhang X, Li R, Wang J (2017) Analysis of grinding mechanics and improved predictive force model based on material-removal and plastic-stacking mechanisms. Int J Mach Tools Manuf 122:81–97. https://doi.org/10.1016/j.ijmachtools.2017.06.002
27. Setti D, Ghosh S, Rao PV (2017) A method for prediction of active grits count in surface grinding. Wear 382-383:71–77. https://doi.org/10.1016/j.wear.2017.04.012